Single-Cell RNA Sequencing of the Primary Visual Cortex in Mice With Optic Nerve Injury

Deling Li,[1] Bin Zou,[2] Qinyuan Hu,[1] Xinyi Zhang,[1] Weiting Zeng,[1] Liling Liu,[1] and Minbin Yu[1]

[1]State Key Laboratory of Ophthalmology, Zhongshan Ophthalmic Center, Sun Yat-Sen University, Guangdong Provincial Key Laboratory of Ophthalmology and Visual Science, Guangzhou, Guangdong, China
[2]Guangdong Provincial Key Laboratory of Major Obstetric Diseases, The Third Affiliated Hospital of Guangzhou Medical University, Guangzhou, Guangdong, China

Correspondence: Minbin Yu, State Key Laboratory of Ophthalmology, Zhongshan Ophthalmic Center, Sun Yat-Sen University, Guangdong Provincial Key Laboratory of Ophthalmology and Visual Science, Guangzhou, Guangdong 510060, China; yuminbin@mail.sysu.edu.cn.

Received: November 27, 2024
Accepted: April 19, 2025
Published: May 23, 2025

Citation: Li D, Zou B, Hu Q, et al. Single-cell RNA sequencing of the primary visual cortex in mice with optic nerve injury. *Invest Ophthalmol Vis Sci.* 2025;66(5):31. https://doi.org/10.1167/iovs.66.5.31

Purpose. Glial cells play a critical role in primary visual cortex (V1 region) damage caused by optic nerve injury, but the mechanisms driving progression of V1 region injury and glial cell heterogeneity remain poorly understood. This study aimed to investigate the damage changes in the V1 region of mice after optic nerve crush (ONC) by single-cell RNA sequencing (scRNA-seq).

Methods. Hematoxylin and eosin (H&E) and immunofluorescence staining were used to evaluate the changes of retinal thickness, astrocytes, and microglia in the V1 region after ONC in mice. Single cell suspensions in the V1 region of mice were prepared and analyzed by scRNA-seq with Seurat, cellchat, CytoTRACE in R software. The expression of PTGDS and CRYAB was measured by qPCR, Western blot, and immunofluorescence.

Results. After unilateral ONC, retinal thinning in both eyes and activation of astrocytes and microglia in contralateral V1 region were observed. Genes related to neuroinflammation and apoptosis in the bilateral V1 region were upregulated, and the related pathways included MAPK, TNF, and apoptosis signaling pathways. Notably, the V1 region contralateral to the ONC eye exhibited more pronounced differential gene expression, and the protein expression of neuroinflammation-related genes *Ptgds* and *Cryab* increased. We further investigated the heterogeneity and pseudotime trajectories of astrocytes and microglia, demonstrating the key branches that dominate neuroinflammation.

Conclusions. This study generates an atlas of the V1 region of the mouse brain, highlighting the role of astrocytes and microglia in the damage changes in the V1 region after ONC, and suggesting *Ptgds* and *Cryab* as potential targets to reduce neuroinflammation.

Keywords: single-cell RNA sequencing (scRNA-seq), optic nerve injury, primary visual cortex, glial cell heterogeneity, PTGDS, CRYAB

Optic nerve injury diseases are a group of common ophthalmic disorders characterized by damage or atrophy of the optic nerve, mainly including glaucoma, optic neuritis, and ischemic optic neuropathy. The main pathological features are retrograde degeneration and death of retinal ganglion cells (RGCs), loss of collateral transmission of damaged axons, and Wallerian degeneration.[1] Due to the lack of effective treatments, about half of the patients eventually lose their vision, leading to a decline in quality of life and placing a heavy burden on families and society. Current research on optic nerve damage diseases, such as glaucoma, predominantly focuses on the retina and optic nerve, but emerging evidence suggests that optic nerve injury also impacts higher visual structures.[2] For instance, functional magnetic resonance imaging has shown a reduced response in the corresponding visual cortex after stimulation in patients with glaucoma.[3] Two-photon calcium imaging has revealed extensive reorganizational plasticity in the visual cortex of adult rats and mice after optic nerve crush (ONC).[4] Despite these insights, the initial factors and pathological mechanisms driving these secondary alterations in the V1 region remain unclear. In rodents, the visual cortex is where the visual signals conducted by the RGCs undergo final processing. Visual information is transmitted from the retina to the cerebral cortex in two subcortical pathways: (1) the geniculo-cortical and (2) the colliculo-cortical pathways.[5–7] Thus, studying the mechanisms underlying optic nerve injury should extend beyond the retina and optic nerve and focus on the central pathogenesis, which is crucial for developing effective prevention and treatment strategies.

Neuroinflammation plays a key role in the pathophysiology of many neurodegenerative diseases.[8–11] Additionally, cell death such as apoptosis, pyroptosis, and apoptosis is associated with neuroinflammatory cytokine release.[12,13] Our prior investigations revealed that unilateral ONC induced astrocyte activation and enhanced neuronal pyroptosis in the contralateral V1 region.[14,15] This suggests that neuroinflammation may be involved in the onset and development of damage in the V1 region after ONC, but the underlying intricate molecular biological mechanisms remain poorly delineated, with critical regulatory genes still

unidentified. The cerebral cortex is the most diverse region developed during human evolution[16] and exhibits particularly complex and heterogeneous injury responses. Therefore, it is necessary to identify the pathomechanisms of damage changes in the V1 region after ONC at the pathway or cellular level. Furthermore, the heterogeneity of glial cells associated with neuroinflammation and the specialized intercellular crosstalk in the V1 region after ONC remain underexplored. Thus, a comprehensive single-cell transcriptomic atlas of the primary visual cortex is imperatively needed to precisely reveal the nuanced changes in the various genes, cell compartments, and biological pathways in the disease state.

Single-cell RNA sequencing (scRNA-seq) provides a comprehensive and precise method for studying genetic information at the level of a single cell,[17] enhancing our understanding of cell types and states. The differentiation of neurons and the development of central nervous system (CNS) diseases is a dynamic process. Utilizing scRNA-seq and pseudotime analysis allows for an in-depth exploration of neuronal and glial cells differentiation in disease states, offering a clearer understanding of the molecular mechanisms underlying neurodegenerative processes and neuroinflammation. Currently, there is a lack of studies mapping the primary visual cortex in mice after ONC, and the genetic and molecular changes at the single-cell level remain poorly understood. In this study, we used the classical ONC model to simulate the pathological changes in the adult mouse brain associated with optic nerve injury. The changes of the V1 region at the single-cell level after ONC were investigated by using scRNA-seq to uncover the complex and heterogeneous mechanisms involved in disease development and progression. This study aims to enhance our comprehensive understanding of the mechanisms underlying the optic nerve injury.

Materials and Methods

Mice

Six to 8 week old wild-type C57BL/6J male mice were housed in a standard environment with adequate food and water. All animal procedures were conducted in compliance with the ARVO Statement for the Use of Animals in Vision and Ophthalmic Research.

Animal Model of Optic Nerve Crush

The optic nerve injury was conducted in the left eye, as described in previous reports.[14] Mice were anesthetized by intraperitoneal injections of Avertin (250 mg/kg; T48402, Sigma-Aldrich, USA). The optic nerve of the left eye was exposed carefully and crushed using fine self-closing forceps (0103-N5-PO; Dumont, Switzerland) at 1 to 2 mm behind the optic disc for 5 seconds, ensuring no damage on the ophthalmic artery surrounding the optic nerve. Mice in the control group only underwent optic nerve exposure without crushing. All mice were euthanized and sampled at 4 weeks after ONC or 4 weeks after the sham operation. The V1 region we observed included both monocular and binocular areas. The left V1 region was defined as the ipsilateral V1 region and the right V1 region was defined as the contralateral (because the majority of optic nerve fibers project to the contralateral hemisphere,[5,7] the contralateral V1 region is the primary visual cortex corresponding to the left ONC eye).

Hematoxylin and Eosin and Immunofluorescence Staining

After anesthesia with Avertin (250 mg/kg), mouse eyeballs and brain tissue were carefully removed for fixation. Coronal sections of brain tissue were prepared at 20-µm thickness for immunofluorescence (IF) staining. Sections of the V1 region were selected based on the *Allen Mouse Brain Coronal Atlas* (https://mouse.brain-map.org/static/atlas). We observed astrocytes at layers 1 to 4, microglia at layers 2 to 6b, and PTGDS and CRYAB staining positive cells at layers 1 to 6b in the V1 region (Supplementary Fig. S1). 5-µm sagittal sections of eyeballs were prepared for hematoxylin and eosin (H&E) staining.

The H&E staining was performed using the H&E Staining Kit (G1120; SOLARBIO, China) according to the manufacturer's instructions. Images were acquired with a fully automated whole-slide imaging system (TissueFAXS 7.1, TissueGnostics, Austria). For IF staining, frozen sections were incubated with diluted primary antibodies IBA1 (17198S, 1:1000; Cell Signaling Technology), GFAP (ab254083, 1:1000; Abcam), S100β (ab52642, 1:100; Abcam), CRYAB (ab281561, 1:50; Abcam), and PTGDS (ab182141, 1:200; Abcam) at 4°C overnight. Sections were incubated with the secondary antibodies Alexa Fluor 488 Donkey anti-rabbit IgG (ab150073, 1:500; Abcam), Alexa Fluor 555 Goat anti-chicken IgY (ab150170, 1:500; Abcam) at room temperature in the dark for 2 hours. Coverslips were applied with antifade reagent containing 4,6-diamidino-2-phenylindole (DAPI; 8961S; Cell Signaling Technology). Sections were visualized at a resolution of 1024 × 1024 using a laser scanning confocal microscope (Zeiss LSM 980; Zeiss, Germany) with 8-bit sampling (without using z-stacks), a Plan-Apochromat 20×/0.8 M27 objective, a laser scan micrometer (LSM), with a scan speed of 3, and scan zoom of 1. Laser parameter settings: selected dyes AF488, DAPI, and /or AF555 and set each light path channel to "Best Signal" mode. For visualization of GAFP- and S100β-stained sections, 561 nm (4.91% intensity), 488 nm (7.10% intensity), 405 nm (4.00% intensity) lasers were selected, and the gain of the AF555 channel, the AF488 channel, and the DAPI channel was set to 650 V, 650 V, and 600 V, respectively. To visualize the IBA1-stained section, 488 nm (6.00% intensity) and 405 nm (2.60% intensity) lasers were selected, and the gain of the AF488 channel and the DAPI channel was set to 633 V and 615 V, respectively. To visualize CRYAB- and PTGDS-stained sections, 488 nm (0.80% intensity) and 405 nm (0.80% intensity) lasers were selected, and the gain of the AF488 channel and DAPI channel was set to 580 V and 550 V, respectively. All channels have a digit offset of 0 and a digital gain of 1. The acquisition and processing of all images for each target protein were identical.

In the figures shown in this article, we used the thresholding method to adjust the brightness contrast of the images to show them more clearly. Image J software was used to identify GFAP, S100β, IBA1, PTGDS, and CRYAB staining regions and to calculate positive staining areas.[18–20] The procedure was conducted as follows[21]: Image J software (Image-Color-Split Channels) was used to split the exported image into 3 single-channel 8-bit grayscale images. Each time the image of the corresponding channel was selected, the

Investigative Ophthalmology & Visual Science

threshold was set using the "Default" algorithm to select the positive staining region. We set the measurement parameters (Analyze-Set Measurements) and obtained the positive staining area by checking "limit to threshold," "area," and "Area fraction." Finally, the result was obtained by "Analyze-Measure."

Quantitative Real-Time PCR

Total RNA of brain tissue was extracted using RNAiso Plus (9108; Takara Biomedical Technology, China). The RNA was reverse transcribed using PrimeScript RT reagent Kit (RR047A; Takara Biomedical Technology). Quantitative real-time polymerase chain reaction (qPCR) was performed with TB Green Premix Ex Taq (RR420A; Takara Biomedical Technology) on the Applied Real-Time PCR System (LightCycler 480 Instrument II; Roche, Switzerland). Primer sequences were designed as follows:

CRYAB: 5′- CGGACTCTCAGAGATGCGTT-3′(forward), 5′- TGGGATCCGGTACTTCCTGT-3′ (reverse);
PTGDS: 5′- GAAGGCGGCCTCAATCTCAC-3′ (forward), 5′- CGTACTCGTCATAGTTGGCCTC-3′ (reverse);
GAPDH: 5′-GGAGTCCACTGGCGTCTTCA-3′ (forward), 5′- GTCATGAGTCCTTCCACGATACC-3′ (reverse).

Western Blotting

Brain tissues from the V1 region were collected and total proteins were extracted. Protein samples were separated using a 4% to 20% SurePAGE Bis-Tris gel (M00656; GenScript, China) and transferred to PVDF membranes. Membranes were incubated with primary antibody against CRYAB (ab281561, 1:1000; Abcam), PTGDS (ab182141, 1:5000; Abcam), and β-Tubulin (2146S, 1:1000; Cell Signaling Technology). Secondary antibodies were applied for 1 hour at room temperature. Immunoblots were scanned and analyzed using Image J software.

Single-Cell RNA Sequencing of Mouse Primary Visual Cortex and Quality Control of Single-Cell Sequencing Data

As shown in Figure 1A, mice from the control group (4 weeks after the sham operation) and the ONC group (4 weeks after ONC) were used ($n = 2$). The bilateral V1 regions were removed into pre-cooled tissue preservation solution, resulting in four samples: the left V1 region of ONC (ONC_LV1), the right V1 region of ONC (ONC_RV1), the left V1 region of control (Ctrl_LV1), and the right V1 region of control (Ctrl_RV1). Brain tissues of V1 region were prepared into single-cell suspensions using enzymatic digestion. The single-cell suspensions were subjected to quality control and counting, requiring a cell viability of 85% or more. Subsequently, single-cell barcoded cDNA libraries were constructed and sequenced by Genergy BIO-TECHNOLOGY (China). Quality control was performed using CellRanger and Seurat software, excluding cells with fewer than 200 gene counts or more than 20% mitochondrial gene ratio. According to the 10× Genomics user guide, a doublets rate of 7.5% was used to filter out doublets, and finally 53,058 cells (ONC_LV1: 14281, ONC_RV1: 14462, Ctrl_LV1: 12192, and Ctrl_RV1: 12123) were obtained for subsequent analysis.

Clustering Analysis and Cell Typing

Three thousand representative highly variable genes were selected for dimensionality reduction and clustering. Cells were clustered based on principal component analysis (PCA) scores and the clustering results were visualized using t-Stochastic Neighbor Embedding (t-SNE) and Uniform Manifold Approximation and Projection (UMAP). Cell types were identified based on the expression of marker genes, whereas some cell clusters that could not be identified were named after their highly expressed genes.

Differential Expression Genes and Gene-Set Enrichment Analysis

The "FindAllMarkers" function was used to identify differential expression genes (DEGs) among different samples. DEGs with $|\text{avg\_log2FC}| > 0.25$ and P (adjusted P value) < 0.05 were selected for Gene Ontology (GO) and Kyoto Encyclopedia of Genes and Genomes (KEGG) analysis.

Cell-Cell Communication Analysis

Cell-cell communication in the V1 region was analyzed using cellphoneDB and cellchat.

Subgroup Analysis and Pseudotime Analysis

Astrocytes and microglia were extracted for subgroup analysis. The differentiation trajectory of astrocytes and microglia was predicted using the CytoTRACE package.

Statistical Analysis

Results were represented as mean ± SEM with specific sample size indicated in the context. Graphing and statistical analysis were performed using statistical software Prism (version 7.03; GraphPad Software, USA). Differences between experimental groups were assessed by Student's t-test or 2-way analysis of variance (ANOVA), followed by Bonferroni post hoc multiple comparisons. P values were considered significant for $P < 0.05$.

Results

Changes of Retinal Thickness, Astrocytes, and Microglia in the V1 Region After ONC in Mice

The thickness of retina and ganglion cell complex (GCC) was measured in the control and ONC mice (Figs. 2A–C). Compared with control mice, both retinal thickness and GCC thickness were reduced in both eyes of mice at 4 weeks after ONC, with a more pronounced reduction in the surgical eyes. There was no significant difference in retinal thickness and GCC thickness between the left and right eyes of the control mice. However, ONC mice showed a significant reduction in GCC thickness in the left eye compared to the right eye, whereas there was no significant reduction in retinal thickness.

In the right V1 region, IBA1$^+$ cells, GFAP$^+$ cells, and S100β^+ cells were significantly increased at 4 weeks after ONC. These findings suggested that unilateral ONC may induce the activation of microglia and astrocytes in the

Investigative Ophthalmology & Visual Science

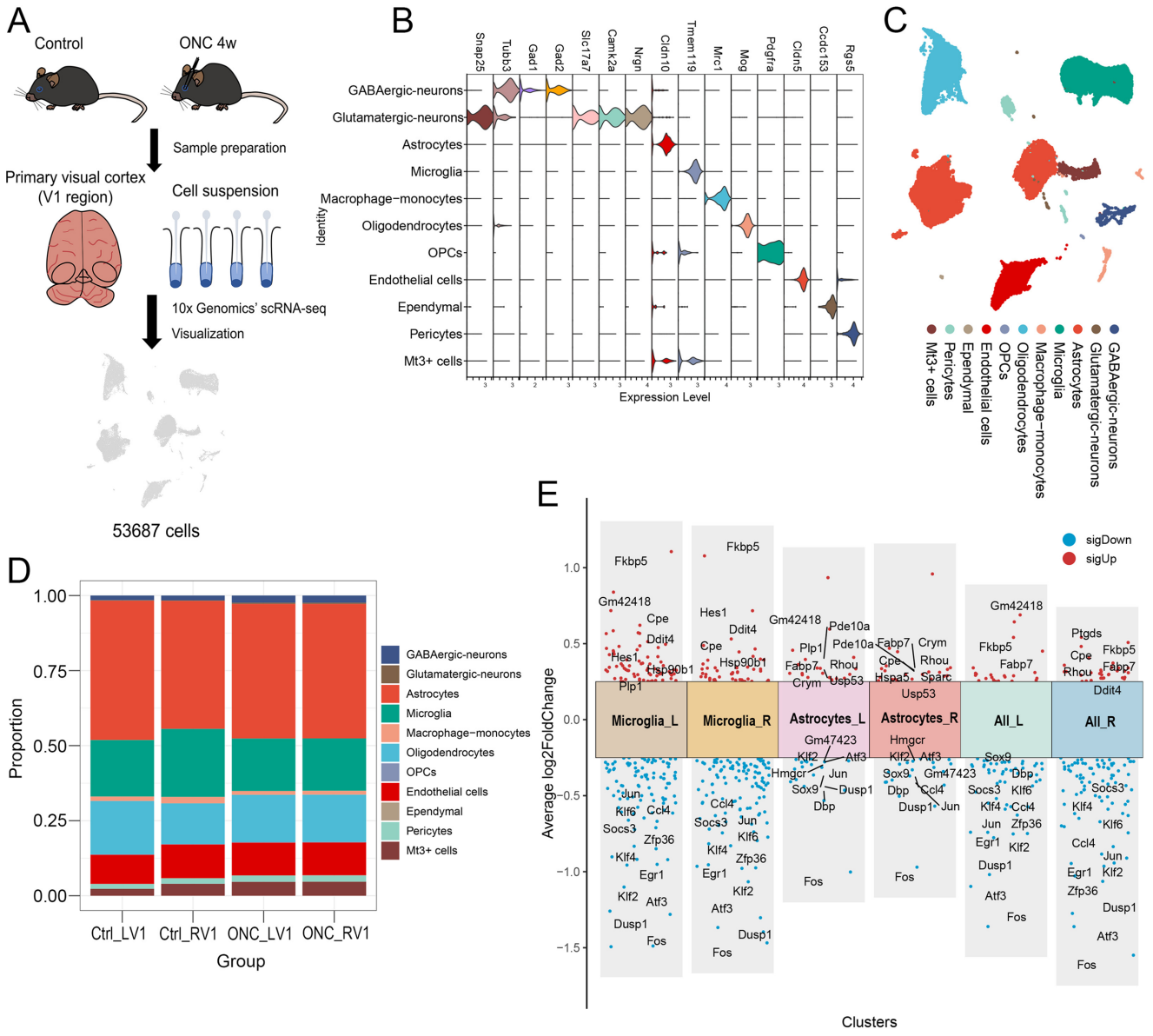

Figure 1. Single-cell atlas of the primary visual cortex of mouse brains. (**A**) Overview of the experimental procedures, including single-cell suspension preparation and sequencing library construction ($n = 2$). (**B**) Seurat stacked violin plot showing expression of marker genes in each cell type. (**C**) Integrative uniform manifold approximation and projection (UMAP) for identifying major cell types based on marker genes of each cluster. (**D**) Histogram of the percentages of all cell types in each sample. (**E**) Systematic differential analysis of gene expression.

contralateral V1 region. Conversely, no significant difference was observed in the ipsilateral V1 region (Figs. 2D–F).

Clustering of Brain Cells in the V1 Region of Mice by scRNA-Seq

Single-cell transcriptome analyses were performed on the control and ONC mice to construct a single-cell atlas of the mouse ONC model. Seurat dimensionality reduction and clustering identified 28 clusters. Cell clusters were annotated according to known marker genes (Fig. 1B). Most cells were well annotated, whereas some clusters that could not be identified were named after their highly expressed genes. Cells in the V1 region were classified into 11 cell types: GABAergic neurons, glutamatergic neurons, astrocytes, microglia, oligodendrocytes, oligodendrocyte precursor cells (OPCs), *Mt3*$^{+}$ cells, macrophage-monocytes, ependymal cells, endothelial cells, and pericytes (Fig. 1C). There was no significant difference in the percentage of all cell types in each sample (Fig. 1D).

Systematic Differential Analysis of Gene Expression

Differential Analysis of Gene Expression in the Right V1 Region Between the ONC Group and the Control Group. Compared to the Ctrl_RV1 group, 34 genes were significantly upregulated (Figs. 1E, 3A; $P < 0.001$) and 84 genes were significantly downregulated (see Figs. 1E, and 3B; $P < 0.001$) in the ONC_RV1 group.

Investigative Ophthalmology & Visual Science

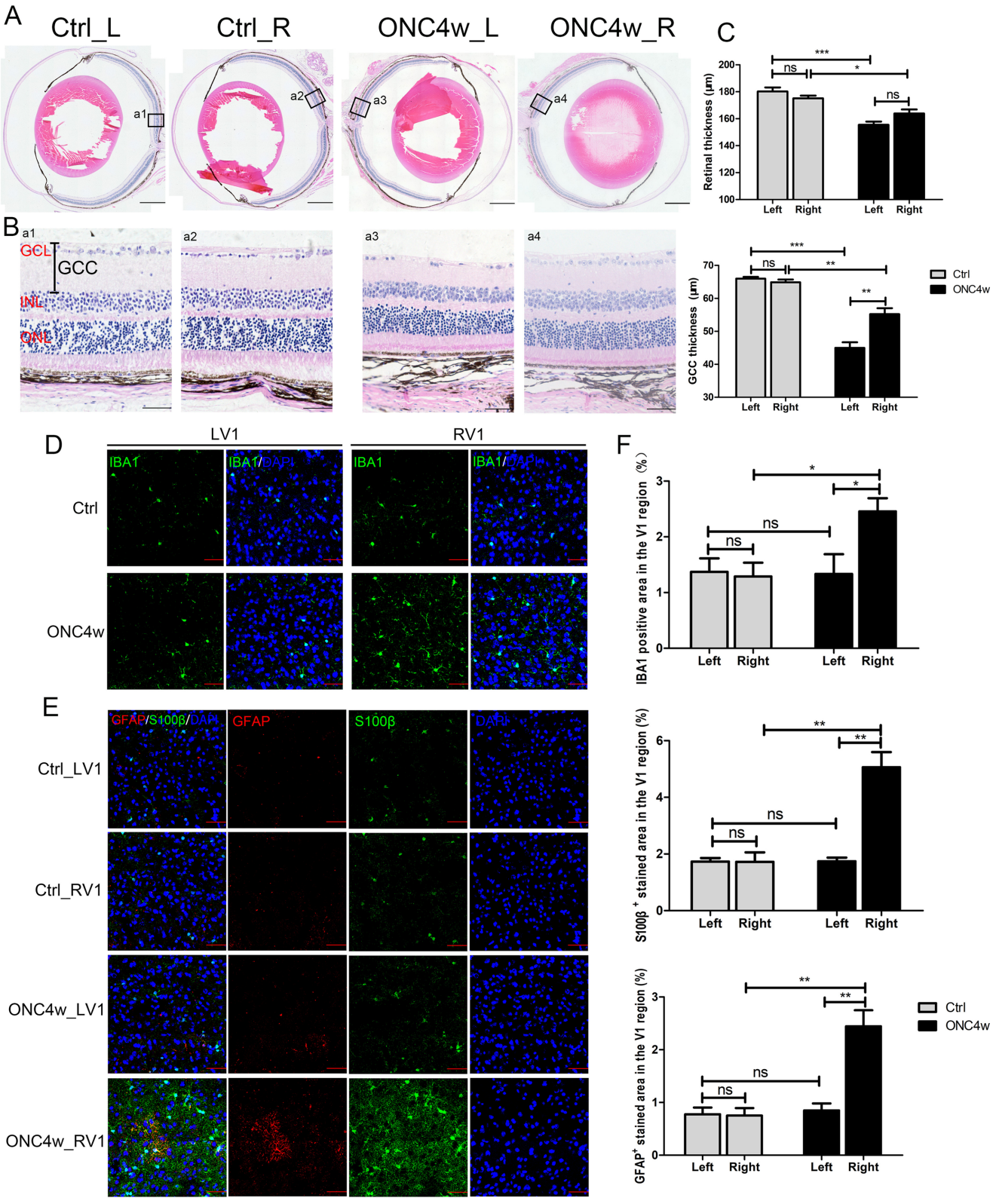

Figure 2. Changes of retinal and GCC thickness in both eyes and activation of microglia and astrocytes in the bilateral V1 region after ONC. (**A**, **B**) H&E staining of mice retinal tissue sections (Bar = A = 500 μm, and B = 50 μm). (**C**) Statistical analysis of retinal thickness and GCC thickness. (**D**, **E**) Expression of IBA1, GFAP, and S100β in the bilateral V1 region in the control and ONC groups (Bar = 50 μm). (**F**) IBA1, GFAP, and S100β staining positive cells and densitometric analysis of immunofluorescence in the bilateral V1 region. GCL, ganglion cell layer; INL, inner nuclear layer; ONL, outer nuclear layer; GCC, ganglion cell complex. Data are mean ± SEM, $n = 4$ animals per group, $^{*}P < 0.05$, $^{**}P < 0.01$, $^{***}P < 0.001$.

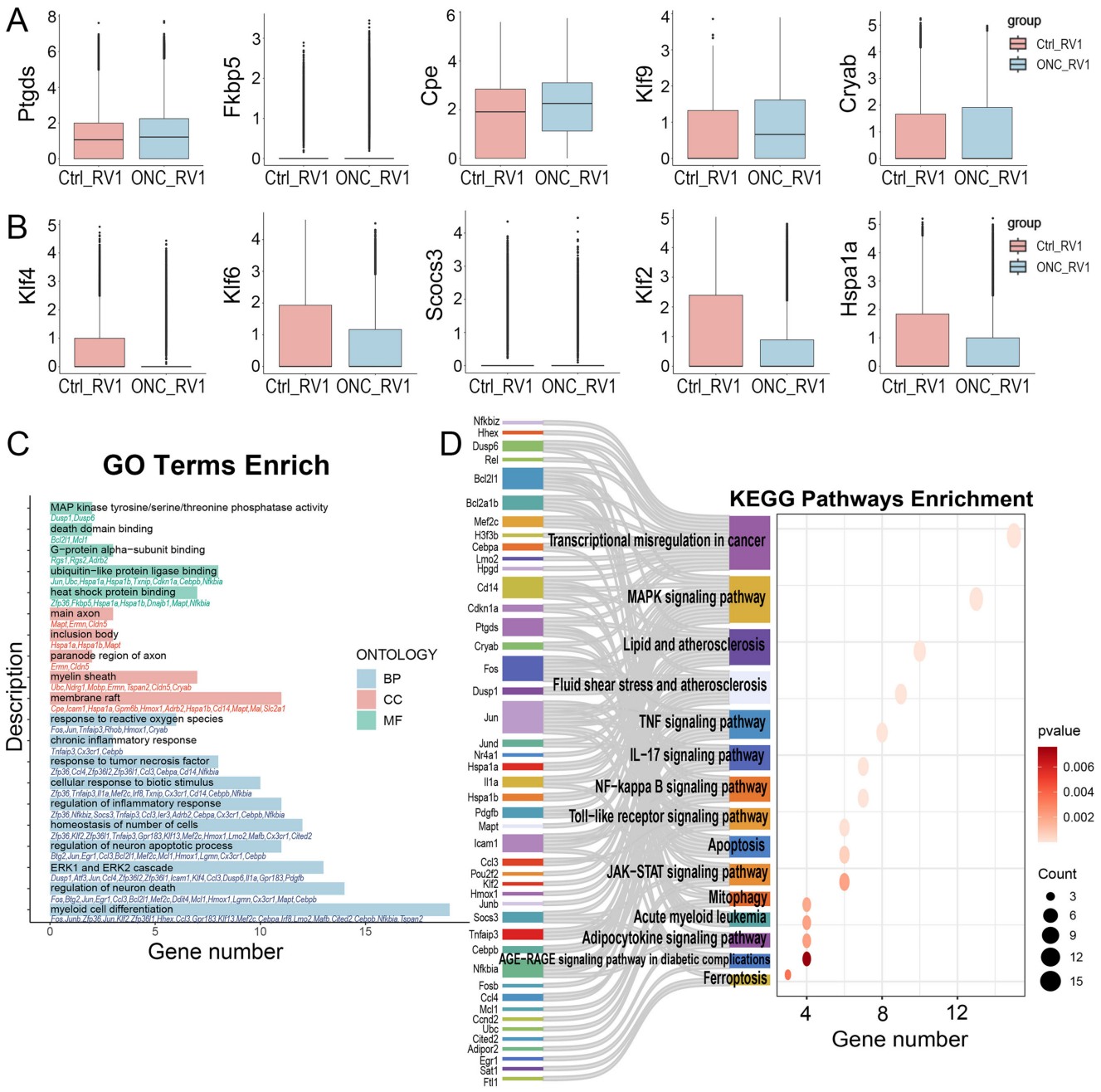

Figure 3. Heterogeneity of the V1 region in the ONC group compared with the control group. (**A**, **B**) Box plots showing the major upregulated (**A**) and downregulated (**B**) genes in the right V1 region in the ONC group compared to the control group. (**C**, **D**) Gene Ontology (GO) and Kyoto Encyclopedia of Genes and Genomes (KEGG) analyses of differential expressed genes (DEGs) with at least 0.25-fold change in the right V1 region of the ONC group compared to the control group.

The vast majority of the upregulated genes were involved in neuronal death and immune inflammation. Top upregulated DEGs included *Ptgds*, which acted as neuromodulators and nutritional trophic factors in the CNS, and was associated with metabolism and neuroinflammation.[22] *Fkbp5* regulated neural excitability and stress response,[23] whereas *Cpe* was implicated in astrocytoma, neurogenesis, and neurodegeneration.[24] *Klf-9* induced cell death and destroyed the dendritic spines of neurons in the brain.[25] *Cryab* was involved in neurodegenerative disorders and neuroinflammatory response.[26] Among the downregulated genes, were *Klf4*, which promoted astrocyte polarization toward A2 subtype through downregulating NF-κB expression,[27] and *Klf6*, which was involved in cell growth and apoptosis.[28] In the ischemia-reperfusion models, KLF6 overexpression reduced inflammation and apoptosis, suggesting a protective role for KLF6 in cell survival.[29] *Socs3* played an important role in CNS regeneration, and its knockdown led to glial cell proliferation and disrupted the balance between macrophage subtypes.[30] *Klf2* was responsible for physiological angiogenesis,[31] and *Hspa1a* was associated with astrocyte phagocytosis.[32] Overall, the genes related to neuroin-

flammation and cell death were significantly upregulated, whereas the genes related to cell protection, repair, and synaptic phagocytosis were significantly downregulated in the contralateral V1 region after unilateral ONC.

The biological significance of these upregulated DEGs was explored by GO and KEGG analysis. These genes were enriched in biological processes mainly related to myeloid cell differentiation, regulation of neuron death, intracellular homeostasis, inflammatory response, and oxidative stress. The pathways involved mainly included MAPK, TNF, IL-17 signaling pathway, apoptosis-related pathway, and ferroptosis (Figs. 3C, 3D). These findings suggested that ONC-induced damaging changes in the right V1 region may be attributed to increased neuroinflammation and impaired neuroprotection.

Differential Analysis of Gene Expression in the Left V1 Region Between the ONC Group and the Control Group. Comparison of DEGs in the ONC_LV1 group and the Ctrl_LV1 group identified 23 upregulated genes associated with neuroinflammation and apoptosis, like *Gm42418*, *AC149090.1*, *Fkbp5*, *Cdkn1a*, and *Fabp7* ($P < 0.001$). A total of 53 genes related to neuronal activation and inflammation regulation, including *Fos*, *Atf3*, *Dusp1*, *Klf2*, and *Egr1*, were significantly downregulated (see Fig. 1E; $P < 0.001$). This meant that ONC could also induce damage responses in the left V1 region.

Similarly, GO and KEGG analyses of these DEGs highlighted that the biological processes' enrichment in ERK1/ERK2 cascade responses, myeloid differentiation, regulation of neuron death, cellular response to external stimulus, and oligodendrocyte differentiation. Key pathways included TNF, IL-17, Toll-like receptor, MAPK signaling pathway, and apoptosis-related pathway (Supplementary Fig. S2).

No significant DEGs were found between the bilateral V1 region in either the control (Ctrl_LV1 versus Ctrl_RV1) or ONC (ONC_LV1 versus ONC_RV1) groups ($P > 0.05$).

PTGDS and CRYAB Were Increased in the Contralateral V1 Region of ONC Mice

Ptgds and *Cryab* were primarily expressed in oligodendrocytes and astrocytes in the V1 region (Fig. 4A). In addition, *Plp*$^+$ astrocyte showed the most significant expression of *Ptgds* and *Cryab* among astrocytes subtypes (Fig. 5D). It was found that mRNA transcription of PTGDS and CRYAB was increased in the contralateral V1 region at 4 weeks after ONC compared to the control group (Fig. 4B). Western blot and immunofluorescence results showed increased expression of PTGDS and CRYAB proteins in the contralateral V1 region after ONC (Figs. 4C–F). These findings, consistent with scRNA-seq results, indicated that the inflammation-related genes *Ptgds* and *Cryab* were upregulated and involved in the damage process in the contralateral V1 region after ONC.

Cell-Cell Communication in the V1 Region of Mice

Differential Analysis of Cell-Cell Communication in the Right V1 Region Between the ONC Group and the Control Group. In general, compared with the Ctrl_RV1 group, the number of cell interactions was less and the strength was weakened in the ONC_RV1 group. After ONC, the number and intensity of interactions among astrocytes and oligodendrocytes, GABAergic-neurons, and *Mt3*$^+$ cells in the right V1 region were increased. Interactions between neurons and microglia were enhanced and the number of interactions among microglia and OPCs, macrophage-monocytes, and Glutamatergic-neurons were increased (Figs. 6A, 6B, 6C). Figures 6D and 6E showed a ligand receptor pair in the interaction of astrocytes, microglia, and other cell types in the Ctrl_RV1 group and ONC_RV1 group. Compared with the Ctrl_RV1 group, the output signals of microglia were attenuated in the ONC_RV1 group, and there was no significant difference in astrocytes. Signals received by astrocytes were decreased, and those received by microglia were increased (Figs. 6F, 6G). As shown in Figure 6H, there were significant differences in the signals of ANGPTL, CSF, ACTIVIN, GAS, and GRN between the Ctrl_RV1 group and ONC_RV1 group. These results suggested that ONC could induce cell-cell communication remodeling in the contralateral V1 region.

Differential Analysis of Cell-Cell Communication in the Left V1 Region Between the ONC Group and the Control Group. Compared to the Ctrl_LV1 group, the number of cell interactions increased and the intensity decreased in the ONC_LV1 group. After ONC, the number and intensity of interactions among astrocytes and ependymal, GABAergic-neurons, *Mt3*$^+$ cells, and OPCs in the left V1 region were increased. The number of interactions among microglia and pericytes, macrophage-monocytes, OPCs, and ependymal were increased (Supplementary Figs. S3A, S3B, S3C). Supplementary Figures S3D and S3E showed ligand-receptor relationships among astrocytes, microglia, and other cell types in the Ctrl_RV1 group and the ONC_RV1 group. Compared with the Ctrl_LV1 group, the output signal of microglia in the ONC_LV1 group was attenuated, and there was no significant difference in astrocytes. The signal received by astrocytes decreased, and the signal received by microglia increased (Supplementary Figs. S3F, S3G). CCL, CHEMERIN, IFN-I, GRN, MK, and other signaling pathways were significantly different between the Ctrl_LV1 group and the ONC_LV1 group (Supplementary Fig. S3H).

Intracellular Heterogeneity and Transcriptomic Changes of Astrocytes in the V1 Region of Mice

As shown in Figures 2D to 2F, we have found that astrocytes and microglia were activated in the contralateral V1 region after ONC. Traditionally, reactive astrocytes were classified into A1 (neurotoxic) and A2 (neuroprotective) subtypes,[33,34] and microglia were classified into 3 subtypes under stimulated conditions: silent, M1 pro-inflammatory, and M2 anti-inflammatory. However, this simplified classification often masked the complex heterogeneity of microglia and astrocytes in various injury or disease conditions.[35–37] Therefore, we reanalyzed astrocytes and microglia isolated from the V1 region to better describe and identify different microglia subtypes and features at the molecular level under optic nerve injury conditions.

Astrocytes were re-clustered into four subpopulations: *Malat1*$^+$ astrocyte (*Malat1*$^+$ astro), *Plp*$^+$ astrocyte (*Plp*$^+$ astro), *Myoc*$^+$ astrocyte (*Myoc*$^+$ astro), and *Zicl*$^+$ astrocyte (*Zicl*$^+$ astro), with each sample containing all subgroups (Fig. 5A). The top 10 differential expression genes analysis identified the characteristics of each cluster (Fig. 5B). *Malat1*$^+$ astro showed high expression of *Malat1*, *Gria2*, *Pnisr*, *Snrnp70*, *Gm26917*, and other genes. These genes were related to anti-inflammatory, anti-apoptotic, and psycho neurodevelopment,[38,39] suggesting that *Malat1*$^+$

Investigative Ophthalmology & Visual Science

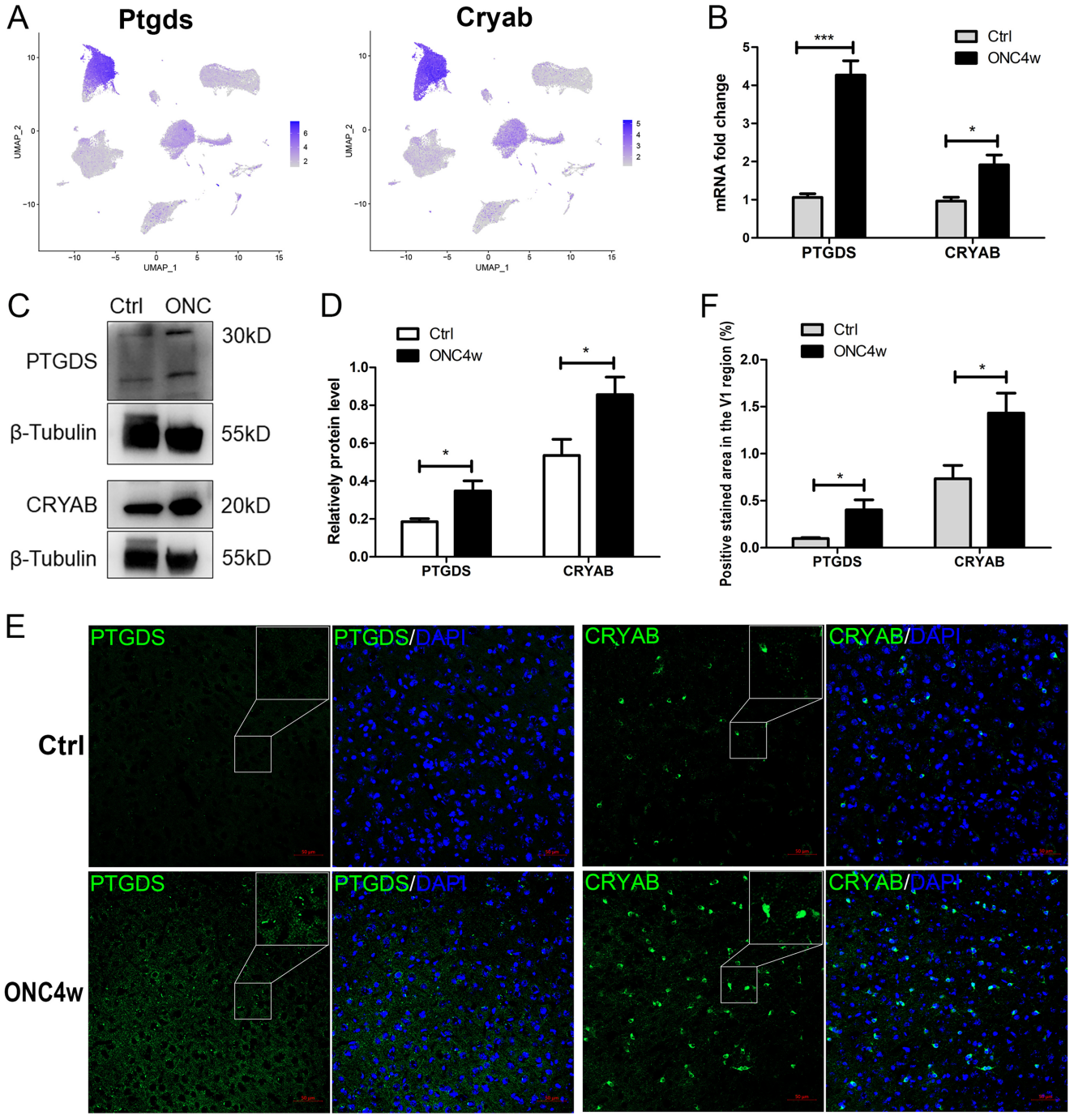

Figure 4. Increased expression of PTGDS and CRYAB in the right V1 region after ONC. (**A**) UMAP plots showing expression of *Ptgds* and *Cryab*. (**B**) The level of expression of PTGDS and CRYAB mRNA in the right V1 region measured by qPCR. (**C**) Western blot analysis of PTGDS and CRYAB expression in the right V1 region. (**D**) Statistical analysis of Western blot for the data shown in (**C**). (**E**, **F**) PTGDS and CRYAB staining positive cells and densitometric analysis of immunofluorescence in the right V1 region (Bar = 50 µm). Data are mean ± SEM, $n = 6$ animals per group, $^{*}P < 0.05$, $^{***}P < 0.001$.

astro may be an anti-inflammatory astrocyte subtype. *Plp*$^{+}$ astro showed high expression of *Plp1*, *Ptgds*, and other genes related to myelin formation, neuronal death, and neuroinflammation.[22] This suggested that *Plp*$^{+}$ astro may be a pro-inflammatory astrocyte subtype. *Myoc*$^{+}$ astro showed high expression of *Myoc*, *Gfap*, *Fxyd6*, *Igfbp5*, *Fbxo2*, *Slc38a1*, and other genes, associated with cell adhesion, proliferation regulation, and tumors.[40] *Slc38a1* is mainly found in undifferentiated neural progenitors,[40] indicating that *Myoc*$^{+}$ astro may be an astrocyte subtype associated with glioma. *Zicl*$^{+}$ astro did not show obvious subtype characteristics and was considered to be in an intermediate state. Notably, we found that *Malat1*$^{+}$ astro was less prevalent and *Plp*$^{+}$ astro was more prevalent in the ONC group (ONC_LV1 and ONC_RV1) compared to the control group (Ctr_LV1 and Ctr_RV1) (Fig. 5C). This indicated that ONC could cause an

Investigative Ophthalmology & Visual Science

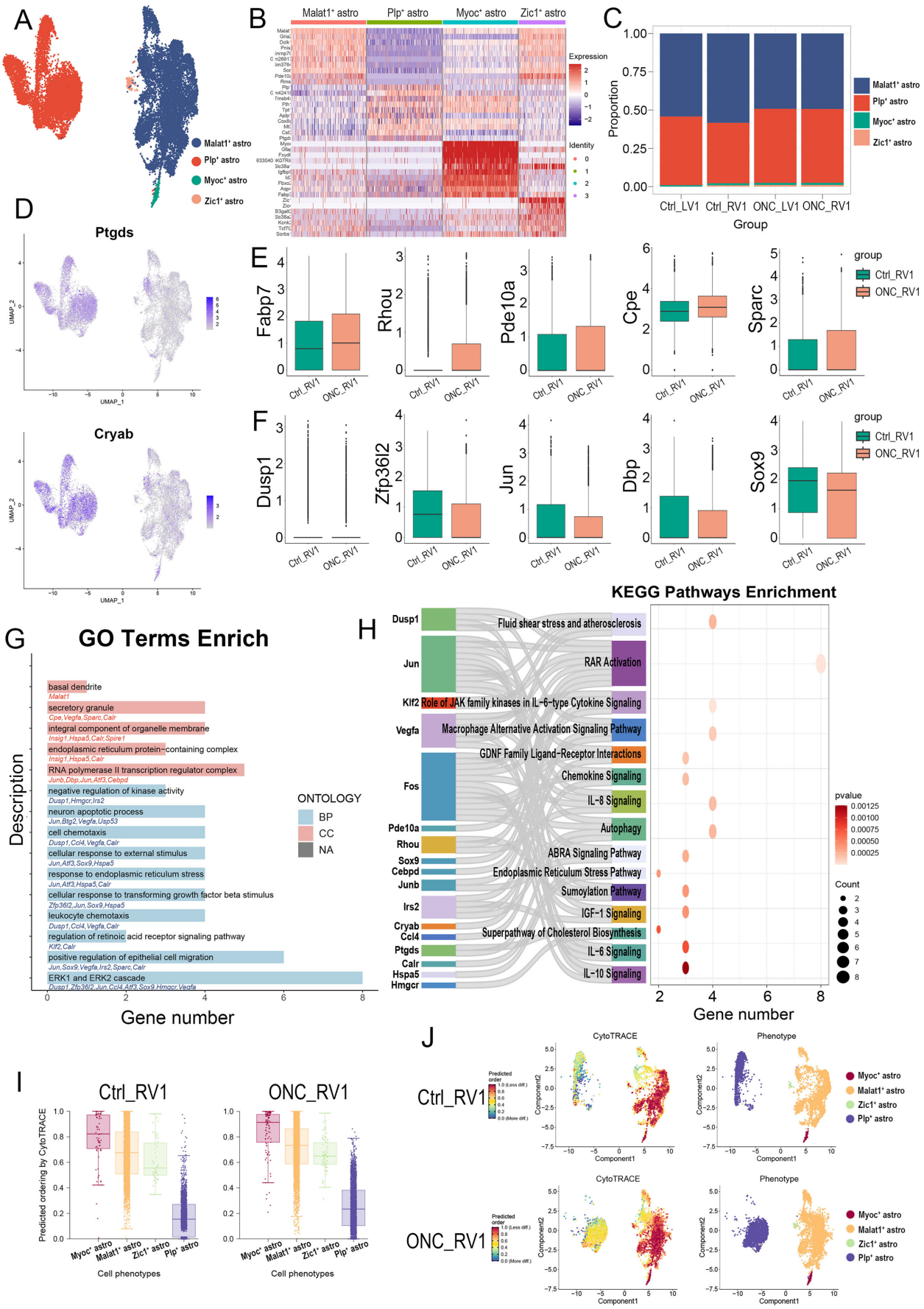

Figure 5. Characterization of astrocyte subtypes. (**A**, **B**) The UMAP plot showing the clustering strategy of astrocyte populations to identify four cell subtypes (**A**), based on the expression heatmap of the top 10 genes in each cluster (**B**). (**C**) Histogram of cell proportions for all

Investigative Ophthalmology & Visual Science

astrocyte subpopulations in each sample. (**D**) UMAP plots of *Ptgds* and *Cryab* expression in astrocytes. (**E**, **F**) Box plots showing major upregulated (**E**) and downregulated (**F**) genes in astrocytes of the right V1 region in the ONC group compared to the control group. (**G**, **H**) GO and KEGG analyses of DEGs with at least 0.25-fold change in astrocytes of the right V1 region in the ONC group compared to the control group. (**I**, **J**) Pseudotime analysis of astrocytes. The sequence of differentiation trajectories is *Plp*$^+$ astro, *Zicl*$^+$ astro, *Malat1*$^+$ astro, and *Myoc*$^+$ astro.

increase in pro-inflammatory astrocytes and a decrease in anti-inflammatory astrocytes in the contralateral V1 region, leading to an amplified inflammatory response.

Comparison of DEGs between astrocytes in ONC_RV1 and those in Ctr_RV1 revealed that 22 significantly upregulated genes, including *Fabp7*, *Rhou*, *Pde10a*, *Cpe*, and *Sparc*, were associated with iron death, atherosclerosis, and neuroinflammation (see Figs. 1E, 5E; $P < 0.001$). Conversely, 20 genes, including *Dusp1*, *Zfp36l2*, *Jun*, *Dbp*, and *Sox9*, related to inflammation regulation, neuronal maturation, and neuronal functional support, were significantly downregulated (see Figs. 1E, 5F; $P < 0.001$). GO and KEGG analysis (Figs. 5G, 5H) revealed that these genes were involved in ERK1/ERK2 cascade responses, epithelial cell migration, cellular response to transforming growth factor stimulation, and neuronal death; and the related pathways mainly included RAR activation, ILK, macrophage alternative activation, chemokine, and IL-8 signaling pathway.

Comparison of the DEGs in ONC_LV1 versus Ctr_LV1 revealed that 22 significantly upregulated genes, including *Gm42418*, *Plp1*, *Pde10a*, *Fabp7*, and *Rhou* ($P < 0.001$). Whereas 18 genes, like *Dbp*, *Zfp36l2*, *Jun*, *Sox9*, and *Hmgcr*, were significantly downregulated (see Fig. 1E; $P < 0.001$). These genes were associated with inflammation regulation and neuronal homeostasis. GO and KEGG analysis showed these genes were mainly related to the ERK1/ERK2 cascade, cellular response to external stimulus, cellular response to transforming growth factor stimulation, neuron apoptotic process, and secretory granule; with pathways mainly including RAR activation, IL-17A, macrophage alternative activation, myelination signaling pathway, and superpathway of cholesterol biosynthesis.

During physiological states or disease development, the states in which cells are located were not completely synchronized. Therefore, using CytoTRACE for temporal sequence analysis, the differentiation trajectory of astrocyte subgroups in ONC group and control group was predicted as follows: *Plp*$^+$ astro, *Zicl*$^+$ astro, *Malat1*$^+$ astro, and *Myoc*$^+$ astro. Combining the highly expressed genes of each cluster, *Plp*$^+$ astro (pro-inflammatory) appeared earlier, and *Zicl*$^+$ astro is the astrocyte subtype in a transitional state, whereas *Malat1*$^+$ astro (anti-inflammatory) and *Myoc*$^+$ astro (related to glioblastoma) appeared later (Figs. 5I, 5J).

Intracellular Heterogeneity and Transcriptomic Changes of Microglia in the V1 Region of Mice

Five distinct microglial subgroups were identified through reclustering: *Tmsb4x*$^+$ microglia (*Tmsb4x*$^+$ micro), *Clu*$^+$ microglia (*Clu*$^+$ micro), *Malat1*$^+$ microglia (*Malat1*$^+$ micro), *Ifit3*$^+$ microglia (*Ifit3*$^+$ micro), and *Ptprd*$^+$ microglia (*Ptprd*$^+$ micro), with all clusters presented in each sample (Fig. 7A). Based on the top 10 differential genes (Fig. 7B), we found that the pro-inflammatory responses and immune activation genes, such as *Nfkbia*, *Egr1*, *Ccl3*, *Fos*, and *Tmsb4x*, were slightly higher expressed in *Tmsb4x*$^+$ micro.[41,42] However, because the differential fold changes were not particularly marked, we speculated that *Tmsb4x*$^+$ micro might be intermediate microglia biased toward pro-inflammatory effects. Genes related to inflammatory regulation, protrophic factors, pro-synaptogenesis, metabolic activity, and proliferation, such as *Igf1*, *Sparcl1*, *Cspg5*, *Clu*, *Ptn*, *Acsl3*, and *Tpi1*, were predominantly overexpressed in *Clu*$^+$ micro.[43–46] Whereas inflammation-related genes, like *Atif3* and *Nfkbia*, were reduced, suggesting that *Clu*$^+$ micro may be associated with anti-inflammatory and protrusion formation. In *Malat1*$^+$ micro, no significantly high or low expressed genes were found, but developmentally related genes, such as *Arhgap* and *Tmem176b*, were expressed,[47] suggesting that *Malat1*$^+$ micro may be undifferentiated embryonic microglia. *Ifit3*$^+$ micro exhibited high expression of genes related to neuroinflammation and brain injury, including *Lgals3*, *Ccl12*, *Ifitm3*, and *Isg15*,[48] suggesting that *Ifit3*$^+$ micro may be a class of pro-inflammatory microglia involved in neurodegeneration. In *Ptprd*$^+$ micro, genes like *Ptprd*, *Mag*, *Mobp*, and *Apod*, which were related to synaptic growth, brain injury regulation, and myelin structure and function, were highly expressed,[49,50] indicating that *Ptprd*$^+$ micro may be a class of microglia related to myelin and neuronal damage repair. In ONC_RV1, the percentage of *Ptprd*$^+$ micro was slightly elevated, whereas *Tmsb4x*$^+$ micro and *Malat1*$^+$ micro were slightly decreased compared to Ctr_RV1. Compared to Ctr_LV1, the percentage of *Clu*$^+$ micro increased and *Tmsb4x*$^+$ micro decreased slightly in ONC_LV1 (Fig. 7C). This suggested a decrease in pro-inflammatory microglial and an increase in anti-inflammatory and pro-repair microglial increased in the bilateral V1 region at 4 weeks after ONC.

Comparing DEGs in ONC_RV1 versus Ctr_RV1, there were 47 genes associated with the regulation of neuronal excitability and stress response, Alzheimer's disease, autophagy, and neuroinflammation, such as *Fkbp5*, *Hes1*, *Ddit4*, *Cpe*, and *Hsp90b1*, were significantly upregulated (see Figs. 1E, 7D; $P < 0.001$). Conversely, 117 genes, such as *Fos*, *Dusp1*, *Klf2*, *Zfp36*, and *Egr1*, related to neuronal activity and inflammation regulation, were downregulated (see Figs. 1E, 7E; $P < 0.001$). GO and KEGG analysis (Figs. 7F, 7G) revealed that these genes were involved in biological processes related to the regulation of cell-cell adhesion, negative regulation of cell activation, response to endoplasmic reticulum stress, ERK1/ERK2 cascade, and myeloid cell differentiation. The enriched pathways mainly included TNF, IL-17, MAPK signaling pathway, apoptosis, and Ferroptosis.

Comparing DEGs in ONC_LV1 versus Ctr_LV1 revealed that 75 genes, including *Fkbp5*, *Gm42418*, *Slc1a2*, *Cpe*, and *Ddit4*, were significantly upregulated ($P < 0.001$). Conversely, 102 genes, like *Fos*, *Klf4*, *Dusp1*, *Klf2*, and *Egr1*, were significantly downregulated (see Fig. 1E; $P < 0.001$). Similarly, these genes were associated with neuronal activity, inflammation regulation, and synaptogenesis. GO and KEGG analysis highlighted biological processes, such as positive regulation of neuron death, negative regulation of phosphorylation, cellular cation homeostasis, regulation of cell-cell adhesion, and ERK1/ERK2 cascade. The enriched pathways

Investigative Ophthalmology & Visual Science

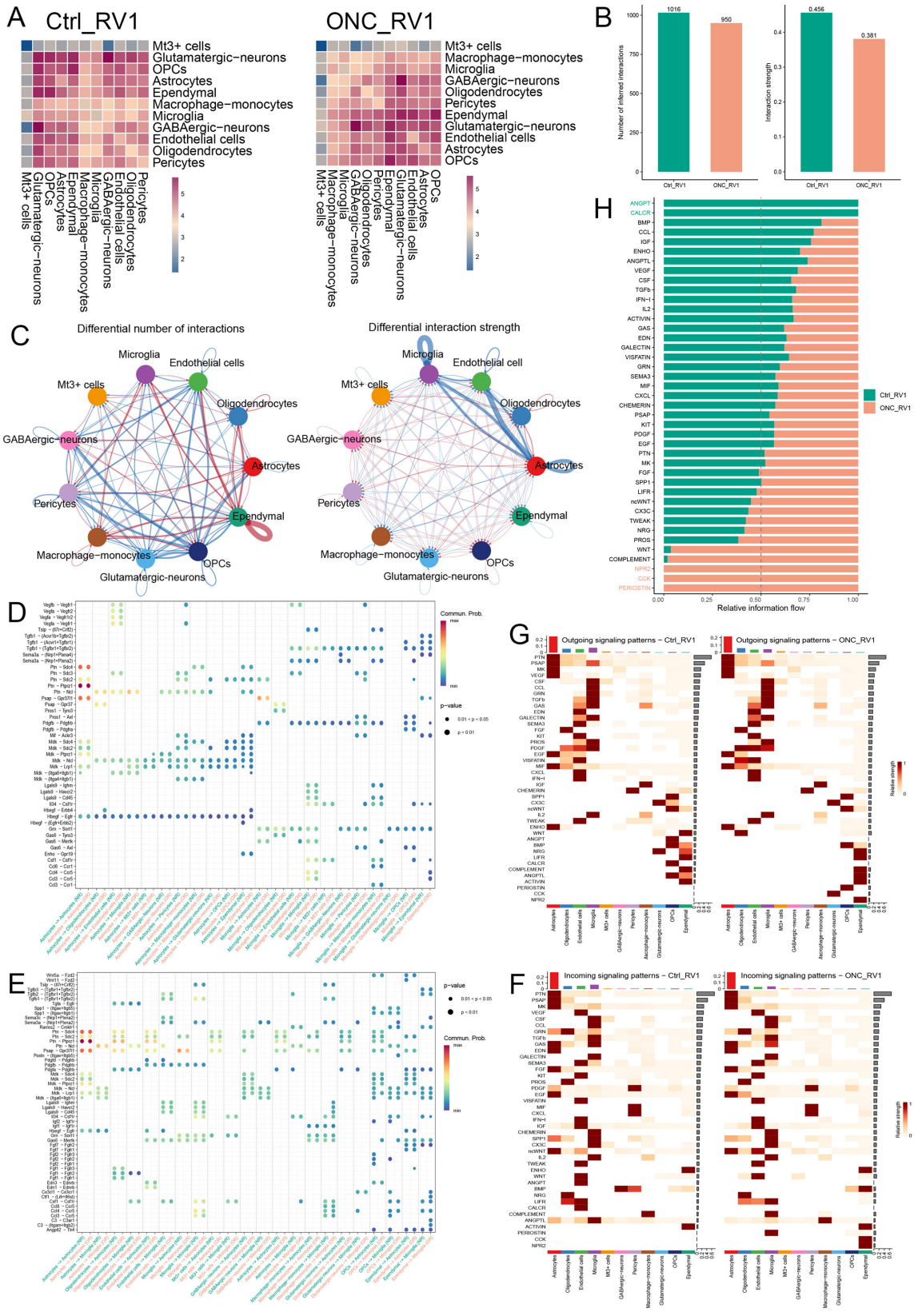

Figure 6. Cell-cell communication in the Ctrl_RV1 group and ONC_RV1 group. (**A**) Heatmap showing the strength of communication connections between cell types in the Ctrl_RV1 group and the ONC_RV1 group. (**B**, **C**) Circular plots and bar plots showing differences in the number and strength of cell interactions between the ONC_RV1 group and the Ctrl_RV1 group. (**D**, **E**) Bubble diagram of ligand receptor pair in interaction of astrocytes, microglia, and other cell types in the Ctrl_RV1 group and the ONC_RV1 group. (**F**, **G**) Incoming and outgoing signaling patterns in the Ctrl_RV1 group and the ONC_RV1 group. (**H**) Bar chart for comparative analysis of signal intensity between the Ctrl_RV1 group and the ONC_RV1 group.

Investigative Ophthalmology & Visual Science

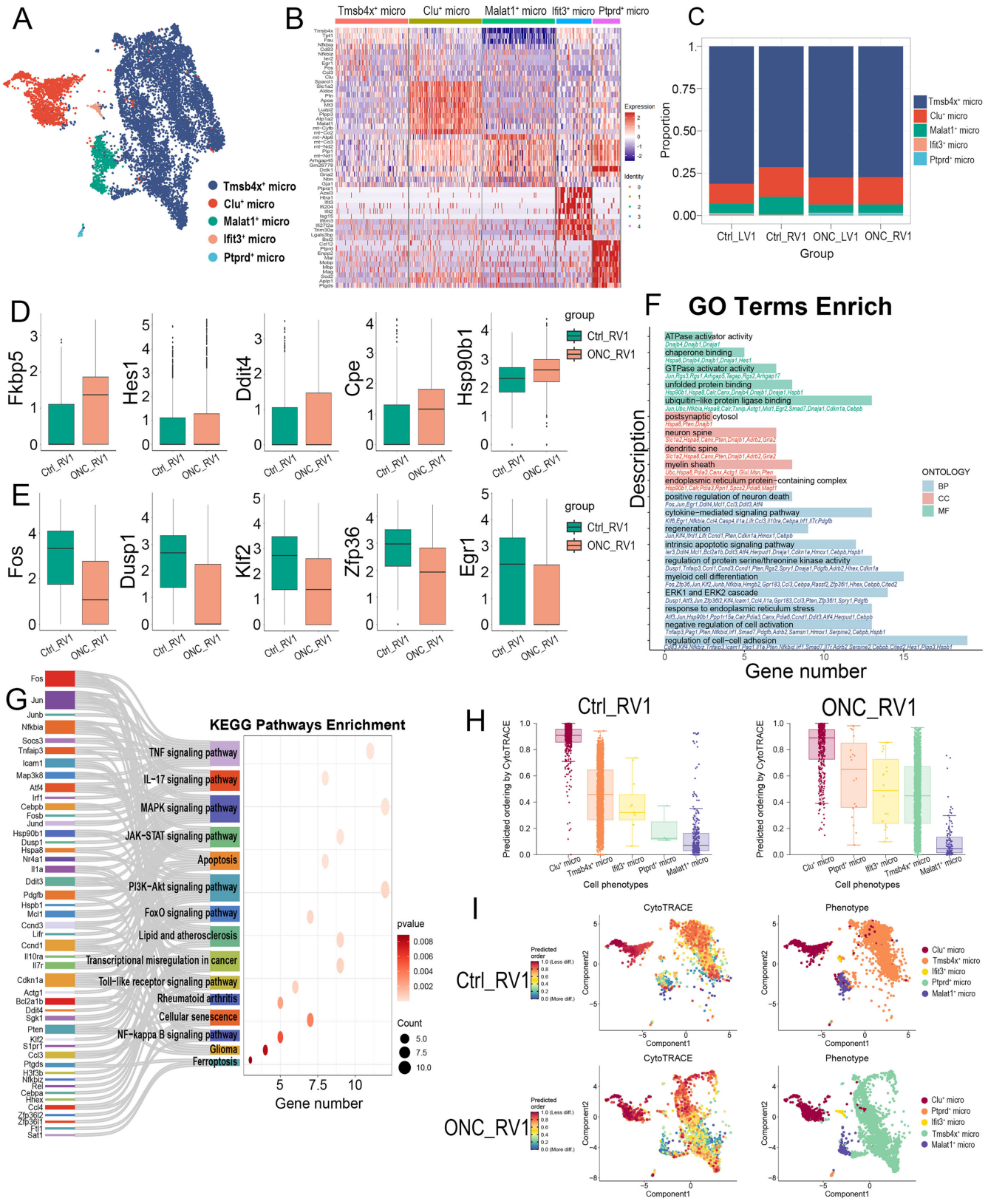

Figure 7. Characterization of microglia subtypes. (**A**, **B**) The UMAP plot showing the clustering strategy of microglia populations to identify five cell subtypes (**A**), based on the expression heatmap of the top 10 genes in each cluster (**B**). (**C**) Histogram of cell proportions for all microglia subpopulations in each sample. (**D**, **E**) Violin plots showing the major upregulated (**D**) and downregulated (**E**) genes in microglia of the right V1 region in the ONC group compared to the control group. (**F**, **G**) GO and KEGG analyses of DEGs with at least 0.25-fold change in microglia of the right V1 region in the ONC group compared to the control group. (**H**, **I**) Pseudotime analysis of microglia. The sequence of differentiation trajectories in control group is *Malat1*$^{+}$ micro, *Ptprd*$^{+}$ micro, *Ifit3*$^{+}$ micro, *Tmsb4x*$^{+}$ micro, and *Clu*$^{+}$ micro. The sequence of differentiation trajectories in ONC group is *Malat1*$^{+}$ micro, *Ifit3*$^{+}$ micro, *Tmsb4x*$^{+}$ micro, *Ptprd*$^{+}$ micro, and *Clu*$^{+}$ micro.

Investigative Ophthalmology & Visual Science

mainly included IL-10, macrophage selective differentiation, MAKP, TNF signaling pathway, and apoptosis.

CytoTRACE analysis predicted the development sequence of microglial subtypes in the control group as follows: *Malat1*$^+$ micro, *Ptprd*$^+$ micro, *Ifit3*$^+$ micro, *Tmsb4x*$^+$ micro, and *Clu*$^+$ micro. Whereas the development sequence of microglial subtypes in the ONC group was as follows: *Malat1*$^+$ micro, *Ifit3*$^+$ micro, *Tmsb4x*$^+$ micro, *Ptprd*$^+$ micro, and *Clu*$^+$ micro. This suggested that *Malat1*$^+$ micro (undifferentiated embryonic microglia) appeared at an early stage, followed by *Ifit3*$^+$ micro (pro-inflammatory) and *Tmsb4x*$^+$ micro (intermediate microglia with a biased pro-inflammatory role), and *Ptprd*$^+$ micro (related to myelin and neuronal damage repair), and *Clu*$^+$ micro (anti-inflammatory) appeared later in the ONC group (Figs. 7H, 7I).

Discussion

Consistent with previous research, we observed that ONC resulted in significant thinning of retinal thickness and GCC thickness in the injured eye, and substantial activation of microglia and astrocytes in the right V1 region. Next, we used scRNA-seq technology to further explore the molecular mechanisms of neuroinflammation caused by glial cells after ONC. We draw the single-cell atlas of the V1 region in both normal and ONC mice, identifying 11 major cell types: GABAergic neurons, glutamatergic neurons, astrocytes, microglia, oligodendrocytes, OPCs, *Mt3*$^+$ cells, macrophage-monocytes, ependymal cells, endothelial cells, and pericytes. This cellular composition closely mirrors that reported for the mouse cerebral cortex.[51] Comparative analysis between control and ONC mice revealed no new cell types or significant changes in cell proportions in the V1 region post-injury. This indicates that the effect of the optic nerve injury on cell classification is microscopic and does not lead to a serious imbalance in cell proportions.

DEGs analysis showed that genes associated with neuroinflammation and cell death were significantly upregulated in the contralateral V1 region at 4 weeks after ONC. Whereas genes related to cell protection, repair, and synaptic phagocytosis showed significant downregulation. Notably, the upregulation of *Ptgds* and *Cryab*, which were closely related to neuroinflammation and neurodegenerative diseases, aroused our interest. PTGDS and CRYAB mainly existed in astrocytes and oligodendrocytes in the CNS, and overexpression of their genes were found to play a key role in neuronal death and neuroinflammation.[26,52] Reducing PTGDS expression could reduce the activation of astrocytes.[53] Similarly, in our study, we observed that the pro-inflammatory subtype *Plp*$^+$ astro overexpressed *Ptgds* and *Cryab*, suggesting these genes may be involved in neuroinflammation. Moreover, our results confirmed increased mRNA transcription and protein expression of PTGDS and CRYAB in the contralateral V1 region at 4 weeks after unilateral ONC, consistent with scRNA-seq results. These findings imply that the inflammation-related genes *Ptgds* and *Cryab* may play roles in the neuroinflammatory response in the V1 region after ONC, but specific molecular mechanisms require further investigation. Similarly, genes related to neuroinflammation and cell death were upregulated and genes related to neuronal protection and inflammation regulation were downregulated in the ipsilateral V1 region after ONC. No significant DEGs were observed between the right and left V1 regions of the control and ONC mice. Our findings suggest that unilateral ONC triggers damage changes in the bilateral V1 region. This contrasts with previous studies, which have shown that unilateral ONC can cause degenerative changes in neurons and astrocyte activation in the contralateral V1 region, but no significant changes in the ipsilateral side.[14,15] We hypothesize that this discrepancy may arise from the fact that most RGCs project to the contralateral side,[5,7] so the changes in the ipsilateral side are not as pronounced as those in the contralateral side. But scRNA-seq is characterized by high resolution and precision, so it can capture subtle cellular changes that cannot be detected by traditional methods. Enrichment analysis of DEGs provides insights into the biological processes and related pathways involved in damage changes of the V1 region after ONC, guiding future research directions.

Through the analysis of cell-cell communication, we found that after ONC, astrocytes closely interacted with ependymal cells, GABAergic-neurons, and *Mt3*$^+$ cells. Whereas microglia were closely related to OPCs and macrophage-monocytes. This suggests that astrocytes and microglia play critical roles in the immune microenvironment of the V1 region after ONC. Signaling pathways, such as ANGPTL, CSF, ACTIVIN, GAS, and GRN, can serve as targets for further studies of the effects of ONC on cellular interactions.

Given the central role of microglia and astrocytes in CNS diseases, our study focused on glial cells activated in the contralateral V1 region after optic nerve injury. Due to variations in gene expression, physiological sensitivity, and gliotransmitter release,[54] glial cells exhibited regional and cellular diversity. We conducted a detailed subtype analysis of astrocytes and microglia, revealing heterogeneity beyond traditional classifications. This analysis enhances our comprehension of their different functions in the local microenvironment.

We identified four subtypes of astrocyte: the anti-inflammatory subtype *Malat1*$^+$ astro, the pro-inflammatory subtype *Plp*$^+$ astro, the glioma-associated subtype *Myoc*$^+$ astro, and the intermediate subtype *Zic1*$^+$ astro. We observed a decrease in *Malat1*$^+$ astro and an increase in *Plp*$^+$ astro in the V1 region of the ONC group compared with the controls, indicating that astrocytes were transformed into pro-inflammatory subtypes following ONC. Microglia were classified into five subtypes, including the intermediate state subtype *Tmsb4x*$^+$ micro with pro-inflammatory effect; the subtype associated with anti-inflammatory and synaptic formation *Clu*$^+$ micro; the undifferentiated embryonic subtype *Malat1*$^+$ micro; the pro-inflammatory, pro-neuronal degeneration, and death subtype *Ifit3*$^+$ micro; and the neuronal injury and repair-related subtype *Ptprd*$^+$ micro. DEGs analysis suggested an inflammatory response in the ONC group. GO and KEGG analysis demonstrated biological processes and pathways involved in astrocytes and microglia, providing a theoretical foundation for investigating their roles in the V1 region after ONC. The results of pseudotime analysis revealed that both astrocytes and microglia exhibited earlier appearances of pro-inflammatory subtypes and later appearances of anti-inflammatory subtypes in the ONC group. These findings enhance our understanding of the roles of glial cells in the V1 region after optic nerve injury, and provide a theoretical basis and direction for regulating glial cells differentiation in future studies.

In summary, scRNA-seq has provided detailed insights into damage alterations and molecular signaling pathways

Investigative Ophthalmology & Visual Science

involved in the bilateral V1 region after unilateral ONC at a single-cell level. Inflammation-related genes *Ptgds* and *Cryab* may serve as potential targets for damage repair. Understanding the heterogeneity and differentiation trajectories of astrocytes and microglia is essential for mitigating neuroinflammation by modulating glial subtype balance in the future.

Acknowledgments

Supported by the National Natural Science Foundation of China (Grant Nos. 81870655, 82271115, and 82471115).

Author Contributions: Minbin Yu: designed the research; Deling Li, Qinyuan Hu, Xinyi Zhang, Weiting Zeng, and Liling Liu: performed the experiments; Deling Li and Bin Zou: analyzed the data; Deling Li: wrote the paper; Minbin Yu and Bin Zou: reviewed and edited the paper.

Ethics Approval and Consent to Participate: Experimental animals were handled in accordance with protocols approved by the Institutional Animal Care and Use Committee of Zhongshan Ophthalmic Center, Sun Yat-Sen University.

Availability of Data and Materials: All datasets used and/or analyzed during this study are available from the corresponding author on reasonable request.

Disclosure: **D. Li**, None; **B. Zou**, None; **Q. Hu**, None; **X. Zhang**, None; **W. Zeng**, None; **L. Liu**, None; **M. Yu**, None

References

1. Torriglia A, Jaadane I, Lebon C. Mechanisms of cell death in neurodegenerative and retinal diseases: common pathway? *Curr Opin Neurol*. 2016;29:55–60.
2. Zhang Z, Liu W, Huang Y, et al. NLRP3 deficiency attenuates secondary degeneration of visual cortical neurons following optic nerve injury. *Neurosci Bull*. 2020;36:277–288.
3. Fiedorowicz M, Dyda W, Rejdak R, Grieb P. Magnetic resonance in studies of glaucoma. *Med Sci Monit*. 2011;17:RA227–RA232.
4. Vasalauskaite A, Morgan JE, Sengpiel F. Plasticity in adult mouse visual cortex following optic nerve injury. *Cereb Cortex*. 2019;29:1767–1777.
5. Gămănuţ R, Shimaoka D. Anatomical and functional connectomes underlying hierarchical visual processing in mouse visual system. *Brain Struct Funct*. 2022;227:1297–1315.
6. Roth MM, Dahmen JC, Muir DR, Imhof F, Martini FJ, Hofer SB. Thalamic nuclei convey diverse contextual information to layer 1 of visual cortex. *Nat Neurosci*. 2016;19:299–307.
7. Seabrook TA, Burbridge TJ, Crair MC, Huberman AD. Architecture, function, and assembly of the mouse visual system. *Annu Rev Neurosci*. 2017;40:499–538.
8. Cohen J, Mathew A, Dourvetakis KD, et al. Recent research trends in neuroinflammatory and neurodegenerative disorders. *Cells*. 2024;13:511.
9. Botella Lucena P, Heneka MT. Inflammatory aspects of Alzheimer's disease. *Acta Neuropathol*. 2024;148:31.
10. Kwon HS, Koh SH. Neuroinflammation in neurodegenerative disorders: the roles of microglia and astrocytes. *Transl Neurodegener*. 2020;9:42.
11. Teleanu DM, Niculescu AG, Lungu II, et al. An overview of oxidative stress, neuroinflammation, and neurodegenerative diseases. *Int J Mol Sci*. 2022;23:5938.
12. Du HY, Wang R, Li JL, et al. Ligustrazine induces viability, suppresses apoptosis and autophagy of retinal ganglion cells with ischemia/reperfusion injury through the PI3K/Akt/mTOR signaling pathway. *Bioengineered*. 2021;12:507–515.
13. Wan P, Su W, Zhang Y, et al. LncRNA H19 initiates microglial pyroptosis and neuronal death in retinal ischemia/reperfusion injury. *Cell Death Differ*. 2020;27:176–191.
14. Zhan Z, Wu Y, Liu Z, et al. Reduced dendritic spines in the visual cortex contralateral to the optic nerve crush eye in adult mice. *Invest Ophthalmol Vis Sci*. 2020;61:55.
15. Li D, Hu Q, Zhan Z, et al. Increased reactive astrocytes and NLRC4-mediated neuronal pyroptosis in advanced visual structures contralateral to the optic nerve crush eye in mice. *Exp Eye Res*. 2025;251:110235.
16. Han X, Zhou Z, Fei L, et al. Construction of a human cell landscape at single-cell level. *Nature*. 2020;581:303–309.
17. Tang F, Barbacioru C, Wang Y, et al. mRNA-Seq whole-transcriptome analysis of a single cell. *Nat Methods*. 2009;6:377–382.
18. Li S, Fang Y, Zhang Y, et al. Microglial NLRP3 inflammasome activates neurotoxic astrocytes in depression-like mice. *Cell Rep*. 2022;41:111532.
19. Lin YT, Yu Z, Tsai SC, Hsu PH, Chen JC. Neuropeptide FF receptor 2 inhibits capsaicin-induced CGRP upregulation in mouse trigeminal ganglion. *J Headache Pain*. 2020;21:87.
20. Kononenko NL, Claßen GA, Kuijpers M, et al. Retrograde transport of TrkB-containing autophagosomes via the adaptor AP-2 mediates neuronal complexity and prevents neurodegeneration. *Nat Commun*. 2017;8:14819.
21. Ververis K, Marzully S, Samuel CS, Hewitson TD, Karagiannis TC. Qualitative and quantitative analysis of histone deacetylases in kidney tissue sections. *Methods Mol Biol*. 2016;1397:279–289.
22. Chen ZP, Wang S, Zhao X, et al. Lipid-accumulated reactive astrocytes promote disease progression in epilepsy. *Nat Neurosci*. 2023;26:542–554.
23. Debs SR, Rothmond DA, Zhu Y, Weickert CS, Purves-Tyson TD. Molecular evidence of altered stress responsivity related to neuroinflammation in the schizophrenia midbrain. *J Psychiatr Res*. 2024;177:118–128.
24. Jiang D, Liu H, Li T, et al. Agomirs upregulating carboxypeptidase E expression rescue hippocampal neurogenesis and memory deficits in Alzheimer's disease. *Transl Neurodegener*. 2024;13:24.
25. Scobie KN, Hall BJ, Wilke SA, et al. Krüppel-like factor 9 is necessary for late-phase neuronal maturation in the developing dentate gyrus and during adult hippocampal neurogenesis. *J Neurosci*. 2009;29:9875–9887.
26. Liu Y, Zhou Q, Tang M, et al. Upregulation of alphaB-crystallin expression in the substantia nigra of patients with Parkinson's disease. *Neurobiol Aging*. 2015;36:1686–1691.
27. Wang C, Li L. The critical role of KLF4 in regulating the activation of A1/A2 reactive astrocytes following ischemic stroke. *J Neuroinflammation*. 2023;20:44.
28. Raninga PV, Di Trapani G, Vuckovic S, Tonissen KF. Targeted knockdown of DJ-1 induces multiple myeloma cell death via KLF6 upregulation. *Apoptosis*. 2016;21:1422–1437.
29. Li J, Yu D, He C, et al. KLF6 alleviates hepatic ischemia-reperfusion injury by inhibiting autophagy. *Cell Death Dis*. 2023;14:393.
30. Park KW, Lin CY, Lee YS. Expression of suppressor of cytokine signaling-3 (SOCS3) and its role in neuronal death after complete spinal cord injury. *Exp Neurol*. 2014;261:65–75.
31. Min L, Zhong F, Gu L, Lee K, He JC. Krüppel-like factor 2 is an endoprotective transcription factor in diabetic kidney disease. *Am J Physiol Cell Physiol*. 2024;327:C477–C486.

32. Shi X, Luo L, Wang J, et al. Stroke subtype-dependent synapse elimination by reactive gliosis in mice. *Nat Commun*. 2021;12:6943.
33. Liddelow SA, Guttenplan KA, Clarke LE, et al. Neurotoxic reactive astrocytes are induced by activated microglia. *Nature*. 2017;541:481–487.
34. Zamanian JL, Xu L, Foo LC, et al. Genomic analysis of reactive astrogliosis. *J Neurosci*. 2012;32:6391–6410.
35. Escartin C, Galea E, Lakatos A, et al. Reactive astrocyte nomenclature, definitions, and future directions. *Nat Neurosci*. 2021;24:312–325.
36. Jiwaji Z, Tiwari SS, Aviles-Reyes RX, et al. Reactive astrocytes acquire neuroprotective as well as deleterious signatures in response to Tau and Ass pathology. *Nat Commun*. 2022;13:135.
37. Hasel P, Rose IVL, Sadick JS, Kim RD, Liddelow SA. Neuroinflammatory astrocyte subtypes in the mouse brain. *Nat Neurosci*. 2021;24:1475–1487.
38. Zeighami Y, Bakken TE, Nickl-Jockschat T, et al. A comparison of anatomic and cellular transcriptome structures across 40 human brain diseases. *PLoS Biol*. 2023;21: e3002058.
39. Cremer S, Michalik KM, Fischer A, et al. Hematopoietic deficiency of the long noncoding RNA MALAT1 promotes atherosclerosis and plaque inflammation. *Circulation*. 2019;139:1320–1334.
40. Ji J, Shen J, Xu Y, et al. FBXO2 targets glycosylated SUN2 for ubiquitination and degradation to promote ovarian cancer development. *Cell Death Dis*. 2022;13:442.
41. Silvin A, Uderhardt S, Piot C, et al. Dual ontogeny of disease-associated microglia and disease inflammatory macrophages in aging and neurodegeneration. *Immunity*. 2022;55:1448–1465.e1446.
42. Festa BP, Siddiqi FH, Jimenez-Sanchez M, et al. Microglial-to-neuronal CCR5 signaling regulates autophagy in neurodegeneration. *Neuron*. 2023;111:2021–2037.e2012.
43. Taketomi T, Tsuruta F. Mutations in Hevin/Sparcl1 and risk of autism spectrum disorder. *Neural Regen Res*. 2023;18:1499–1500.
44. Liu X, Che R, Liang W, et al. Clusterin transduces Alzheimer-risk signals to amyloidogenesis. *Signal Transduct Target Ther*. 2022;7:325.
45. De Miguel Z, Khoury N, Betley MJ, et al. Exercise plasma boosts memory and dampens brain inflammation via clusterin. *Nature*. 2021;600:494–499.
46. Zhou Y, Li H, Liu X, et al. The combination of quantitative proteomics and systems genetics analysis reveals that PTN is associated with sleep-loss-induced cognitive impairment. *J Proteome Res*. 2023;22:2936–2949.
47. Hammond TR, Dufort C, Dissing-Olesen L, et al. Single-cell RNA sequencing of microglia throughout the mouse lifespan and in the injured brain reveals complex cell-state changes. *Immunity*. 2019;50:253–271.e256.
48. Newcombe EA, Camats-Perna J, Silva ML, Valmas N, Huat TJ, Medeiros R. Inflammation: the link between comorbidities, genetics, and Alzheimer's disease. *J Neuroinflammation*. 2018;15:276.
49. Chibnik LB, White CC, Mukherjee S, et al. Susceptibility to neurofibrillary tangles: role of the PTPRD locus and limited pleiotropy with other neuropathologies. *Mol Psychiatry*. 2018;23:1521–1529.
50. Chen WT, Lu A, Craessaerts K, et al. Spatial transcriptomics and in situ sequencing to study Alzheimer's disease. *Cell*. 2020;182:976–991.e919.
51. Tasic B, Menon V, Thuc Nghi N, et al. Adult mouse cortical cell taxonomy revealed by single cell transcriptomics. *Nat Neurosci*. 2016;19:335–346.
52. Gong L, Gu Y, Han X, et al. Spatiotemporal dynamics of the molecular expression pattern and intercellular interactions in the glial scar response to spinal cord injury. *Neurosci Bull*. 2023;39:213–244.
53. Zhao W, Jiang B, Hu H, et al. Lack of CUL4B leads to increased abundance of GFAP-positive cells that is mediated by PTGDS in mouse brain. *Hum Mol Genet*. 2015;24:4686–4697.
54. Ben Haim L, Rowitch DH. Functional diversity of astrocytes in neural circuit regulation. *Nat Rev Neurosci*. 2017;18:31–41.

Investigative Ophthalmology & Visual Science